Electrical Engineering (2023) 105:4339–4360
https://doi.org/10.1007/s00202-023-01943-y

ORIGINAL PAPER

Cascaded fractional order automatic generation control of a PV-reheat thermal power system under a comprehensive nonlinearity effect and cyber-attack

Bora Cavdar[1] · Erdinc Sahin[2] · Erhan Sesli[3] · Omur Akyazi[1] · F. Mehmet Nuroglu[4]

Received: 5 May 2023 / Accepted: 11 July 2023 / Published online: 5 August 2023
© The Author(s), under exclusive licence to Springer-Verlag GmbH Germany, part of Springer Nature 2023

Abstract
The integration of renewable energy systems into the existing power grid has become a global necessity. While there are numerous advantages to this integration, it also presents challenges such as oscillations in system frequency and tie-line power. These issues can lead to instability and undesirable situations within the power system. To ensure a consistent and reliable supply of high-quality electrical power to consumers, a control system is essential. In recent years, cascaded controllers, known for their increased flexibility and degree of freedom compared to non-cascaded controllers, have gained popularity in the literature. In this study, we aim to examine the performance of cascaded fractional and integer order TI-TD and PI-PD controllers in comparison with non-cascaded PID and TID controllers for a challenging stability and robustness assessment. Our focus is on a two-area PV-reheat thermal power system. By conducting comprehensive tests, we aim to gain insights into the effectiveness of these controller types within this context. To ensure optimal controller responses, the designed controllers are optimized using the Mayfly algorithm, with a focus on minimizing the integral of the time-weighted absolute error performance index. The performance tests conducted in this study cover various aspects, including time domain analysis, robustness, random load changes, the impact of progressive nonlinearities, and cyber-attack (C-A) scenarios. The power system under examination incorporates several nonlinear components, namely governor dead band, generation rate constraints, boiler dynamics, and time delay. Additionally, two C-A models, namely resonance attack (ResA) and random attack, are applied to the controller systems. Unlike conventional robustness and C-A tests found in existing literature, this study goes further by measuring the response of the proposed controller to high parameter changes (uncertainty) and conducting a quantitative analysis of its resilience against C-A scenarios. The aim is to assess the controller's ability to withstand significant variations in system parameters and its effectiveness in dealing with cyber-attacks. The simulation results demonstrate the superior performance of the optimized and cascaded controllers, particularly the TI-TD controller. These controllers exhibit improved performance compared to other controllers reported in the literature. The findings validate the effectiveness of the proposed controllers and highlight their advantages in terms of system stability, response time, and overall control quality.

Keywords TI-TD controller · PI-PD controller · Mayfly algorithm · Cyber-attack · Progressive Nonlinearity effect · Random load change · Two area PV-thermal reheat power system · Robustness and stability toleration limits

Bora Cavdar, Erdinc Sahin, Erhan Sesli, Omur Akyazi, F. Mehmet Nuroglu have contributed equally to this work.

✉ Bora Cavdar
boracavdar@ktu.edu.tr

Erdinc Sahin
erdinc.sahin@giresun.edu.tr

Erhan Sesli
erhansesli@ktu.edu.tr

Omur Akyazi
oakyazi@ktu.edu.tr

F. Mehmet Nuroglu
fmn@ktu.edu.tr

[1] Energy Systems Engineering, Karadeniz Technical University, 61830 Of, Trabzon, Türkiye

[2] Computer Engineering, Giresun University, 28200 Giresun, Türkiye

[3] Electronics and Telecommunication Engineering, Karadeniz Technical University, 61830 Of, Trabzon, Türkiye

[4] Electrical and Electronics Engineering, Karadeniz Technical University, 61080 Trabzon, Türkiye

1 Introduction

1.1 Background

Frequency is one of the main parameters that must be kept within the determined limits in order to provide high-quality electrical power with increased reliability. Due to the disturbances, short-circuit faults, C-As, load-side changes, and integration of renewable energy sources (generation units with inverter) into the electrical grid, instant deviations or long-term oscillations in the frequency response may be encountered [1, 2]. If these oscillations get bigger and bigger over time and are not quickly suppressed, the interconnected power system may become unstable. Thus, the power change in the tie-line and the frequency change in the interconnected power systems should be eliminated or minimized via control systems [3]. Automatic generation control (AGC) or load frequency control (LFC) is used to remain frequency and power flows between the areas at their scheduled values under normal and unexpected conditions.

With the increasing penetration of inverter-based renewable energy sources (e.g., PV plants) in power systems, LFC becomes more challenging. This is due to the difference between synchronous generators and inverter-based generation sources. Synchronous generators are the main component for keeping the frequency of the power system between the desired limits with their moment of inertia and primary frequency support. Inverter-based generation sources challenge power system frequency control due to their lack of moment of inertia and limited capability to provide primary frequency support. This becomes particularly evident when there is an imbalance between generation and consumption. In a power system with a high PV plant penetration rate, a late and inadequate response to this imbalance result (transient event) can lead to system collapse. In order to prevent such scenarios, a comprehensive approach involving various solutions should be adopted within the power system. These solutions encompass the integration of synchronous generators alongside PV plants. For instance, providing frequency support for PV plants and virtual moment of inertia generation are key components of these solutions. Likewise, enhancing controller performance for synchronous generators is another critical aspect to be considered.

1.2 Literature review

A PID controller, even if it is one of the earlier control methods, is still frequently used in industrial control applications today due to its strong dynamic performance, robustness, and easy implementation [4, 5]. It is also called as three-term controller since it has three parameters (proportional constant K_p, integrator constant K_i, and derivative constant K_d) that need to be set properly. It can be easily observed from the literature that the most preferred controller scheme for the AGC problem is the PID controller and its different variations such as cascaded and fractional ones. However, PID controllers may cause larger oscillations and longer settling times under variations in loading conditions, uncertainties, and nonlinearities.

With the advancement of fractional calculus, it is possible to implement the integer order PID controller as fractional. Making the order of the derivative (λ) and integrator (μ) terms of a PID controller fractional results in a fractional order PID controller (FOPID). The new fractional structure provides more design flexibility leading to improvement in the system response and stability. On the other hand, the number of control parameters that need to be optimized has increased to five due to these extra two parameters [6]. Therefore, the process of calculating the optimum value of the controller parameters becomes more complex.

The other well-known fractional order controller structure is the tilt-integral-derivative (TID) controller. A TID controller is similar to a PID controller. Integral and derivative action is the same for both controllers. However, the proportional coefficient in the PID controller K_p was modified in the TID controller and it is replaced with an oblique component consisting of a fractional integrator and a tilt constant (K_t) [7, 8].

Another way to increase the flexibility of a control system is to connect controller types as cascaded. Two notable examples of this method are PI-PD and TI-TD controllers. PI-PD controllers are one of the incremental control approaches used to improve the performance of unstable and integral systems. PI-PD controllers have more set points than PID controllers [9]. TI-TD controller is based on fractional order control and cascade control theory [10, 11]. The TI-TD controller has two control loops and can provide a better closed-loop response to system changes than conventional controllers. Some of the recently introduced cascaded integer and fractional order controller structures used in LFC problems are PI-PD [10, 12–14], FOPI-FOPD [15], TD-TI [16], TI-TD [10], (1+PD)-PID [17], PIDn-PI [18], PD-P-PID [19], PI-PI and PDn-PI [20], (FOPD-(1+FOI)) [21], FOPI-FOPTID [22], and FPIDF-(1+PI) [23].

In order to get the best controller performance, the controller parameters should be tuned properly. Numerical methods, artificial intelligence applications, and meta-heuristic algorithms are frequently used in the optimization process of controllers. Especially, in recent years, meta-heuristic methods have gained high attention because of their fast, reliable, and successful convergence results to the optimal solution. Some of the meta-heuristic algorithms used in AGC problems are given as follows: firefly algorithm (FA) [24], particle swarm optimization (PSO) [25, 26], whale optimization algorithm (WOA) [5], symbiotic organism search algorithm (SOSA) [27], differential search algorithm (DSA)

[28], invasive weed optimization algorithm (IWOA) [29], differential evolution algorithm (DEA) [30], pathfinder algorithm (PA) [31], imperialist competitive algorithm (ICA) [32], hybridization of meta-heuristic algorithms [33, 34], dragonfly search algorithm (DSA) [17], chaos game optimization (CGO) [18], marine predators algorithm (MPA) [19], global neighborhood algorithm (GNA) [22], etc.

For the optimization process, an objective function should be employed. There are many objective functions in the literature for setting controller parameters [35, 36]. The most commons of these are the integral of the time-weighted absolute error (ITAE), the integral of the square of the error (ISE), the integral of the absolute error (IAE), and the integral of the square of the time-weighted error (ISTE) [37]. Among the previously specified objective functions, ITAE has been preferred in most of the AGC studies [13, 16–22]. The reason why it is favored is that it offers a quicker response (settling time) with less damped oscillation (undershoot/overshoot) [37].

In the literature, load frequency control has been researched for a wide variety of power system models. These power systems can be divided into different groups according to the following headings: the number of areas (1, 2, 3, and so on), system type (traditional or deregulated), generation source type (wind, solar, thermal, hydro, nuclear, gas, diesel, etc.), number of the generation source (single or multi), and consideration of the nonlinear effects, the devices of flexible AC transmission systems (FACTS), electrical vehicle (EV), energy storage units, and high voltage DC (HVDC) systems [38]. The number of subtitles can be increased since there are a lot of components for an LFC study. One of these popular power systems is a two-area PV-reheat thermal (PV-RT) power system which is also considered for this study. Due to the benefits of PV systems such as pollution reduction, quiet operation, simplicity in installation, and adaptability, power systems with PV integration become more remarkable. On the other hand, PV integration with nonlinear effects makes it difficult to control the overall power system response and stability. A detailed comparison of the papers that have studied PV-RT power system is given in the following section.

The other hot topic for the LFC studies is also the investigation of the power system response under the different cyber-attack (C-A) models. Cyber security has been the subject of research in power systems recently and has come to the fore with the development of smart grids. Many C-A methods are used in power systems. Some examples of these methods are time-delay switch attack [39], denial-of-service attack [40], resonance attack (ResA) [41] and random attack (RndA) [41].

1.3 Motivation and contributions

The widespread use of inverter-based generation sources (e.g., PV plants) in the power system (negative impact on frequency) and the developments in smart grids are the motivations for this study. Therefore, the PV-RT power system is discussed. Both linear and nonlinear models of the considered PV-RT power system are studied.

According to the literature on the LFC problem stated above, there are several control schemes including linear or nonlinear techniques with and without their cascaded connections. Numerous earlier studies failed to take into account the various difficulties that power systems encounter such as random load change (RLC), C-A performance, and detailed nonlinearity analysis.

In order to improve the stability of the examined system, this study investigates the performance of the cascaded control architectures known as TI-TD and PI-PD controllers which are derived from the classical TID and PID controllers in MATLAB, respectively. The Mayfly algorithm (MA) is employed to determine the parameters of the proposed controllers. The reason to prefer MA in this study is that it provides high convergence performance to the optimal solution and its superiority over the PSO, GA, FA, DE, HSA, IWO, and BA has already been proven [42]. In addition, ITAE has been proven to outperform other objective functions in AGC [43]. For this reason, ITAE is used as an objective function in MA.

The performances of the proposed controllers are taken into account under the threats of C-A (ResA and RndA), load perturbation (SLC and RLC), parameter uncertainty ($\pm 75\%$), nonlinearity (GRC, GDB, TD, and BD). ResA and RndA are chosen as C-A methods because it is difficult to detect [41]. The nonlinear component analysis consists of two stages.

In the first stage, GDB and GRC are taken into account, and in the second stage, the effects of GDB, GRC, BD, and TD are considered. Controller performance for transient response and stability are discussed. In contrast to traditional robustness tests in the literature, this study considers the high rate of parameter change (uncertainty) of the proposed controller. It also quantitatively determines how large a C-A (in different methods) the system (for controllers) can withstand.

To address the shortcomings of previous studies in the literature, this paper addresses several analyses. Table 1 shows the distinguishing features of our study compared to the existing literature on PV-RT power system.

The main contributions of this paper can be summarized item by item as follows.

- Performances of the MA-tuned TI-TD and PI-PD cascade controllers over the MA-tuned TID and PID and other available controllers in literature are discussed in detail for the LFC of a PV-RT power system.

Table 1 The motivation of this study compared to existing papers worked on PV-RT power systems in literature

Ref.no	Pub. year	Controller type	Controller design algorithm	Objective function	Sensitivity analysis and max. limits in considered range of	Load perturb. challenge	Trans. res. perform	Effect of nonl. comp	C-A perform	Stab. lim. analysis
[24]	2018	PI	GA, FA	ITAE	± 40%	SLC	NC	NC	NC	NC
[44]	2018	Fuzzy-PI	ICA	ISE	± 25%	SLC	C	GRC	NC	NC
[45]	2018	Fuzzy-PIDF-II	ICA	ISE	± 25%	SLC	C	GDB	NC	NC
[23]	2019	Fuzzy-PIDF-(1+PI)	ICA	ISE	± 25%	SLC, RLC	C	NC	NC	NC
[5]	2020	PI / PID / PIDF	WOA, MWOA	ITAE	± 40%	SLC	NC	NC	NC	NC
[46]	2020	PI / PID	SFLA, hSFLA-PS	ITAE	± 40%	SLC	NC	NC	NC	NC
[20]	2021	PI / PDF / PI-PI / PDF-PI	ECOA	ITAE	± 40%	SLC, RLC	C	NC	NC	NC
[47]	2022	PI / PID	BWOA	ITAE	± 50%	SLC	C	TD, GRC, GDB	NC	NC
[48]	2022	Fuzzy-PI	PSO	ITSE	NC	SLC, RLC	NC	NC	NC	NC
[49]	2022	PID / TID	GWO-CS, MGWO-CS	ITAE	NC	SLC, RLC	NC	NC	NC	NC
[18]	2023	PI / PIDF / PIDF-PI	PSO, MFO, CGO	ITAE	± 50%	SLC, RLC	C	GRC, TD	NC	NC
[50]	2023	PID	WOA	IAE	NC	SLC, RLC	C	NC	NC	NC
Proposed study		PID / TID / PI-PD / TI-TD	MA	ITAE	± 75%	SLC, RLC	C	GRC, GDB, TD, BD	C	C

NC Not considered, *C* Considered

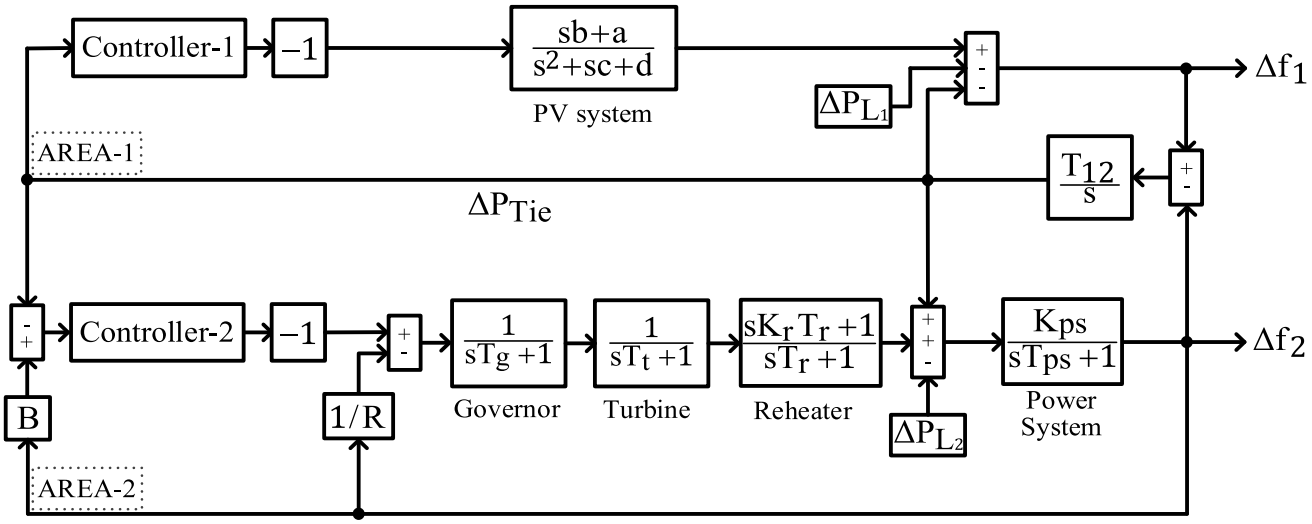


Fig. 1 Linearized model of a two-area PV-RT power system

- A two-stage nonlinear component analysis is considered for the controllers. In this way, a systematical nonlinearity approach is applied to the proposed control systems.
- Effects of two different C-A models (with and without system information) are examined for the first time in a PV-RT power system.
- Unlike the robustness analysis in the literature, the parameter uncertainty change limit is considered as ±75%, and the stability limits for C-As have been determined.

This paper is organized as follows. In Section 2, the methodology is presented with the subtitles: the power system model, nonlinear components, C-A methods, proposed controller structures, and optimization process. Simulation results are given in Section 3. Finally, in Section 4, the conclusion is stated.

2 Methodology

Under this title, the mathematical model of the PV-RT power system, nonlinear components, C-A models, a brief summary of fractional calculus and considered fractional order controllers, and MA with considered objective function are given, respectively.

2.1 PV-thermal reheat power system

In this section, the power system used in this study is explained. In the study, the two-area PV-RT power system is discussed. The model of this system is given in Fig. 1.

In the first area of the two-area power system, there is the PV power plant model. In the second area, there is the reheat thermal power plant model. In this system, two areas are controlled by controllers (Controller-1 and Controller-2) with different parameters, as there are different generation plants in the two areas. The "-1" coefficient in front of the controllers in the system is because cascade controllers are used in the study.

In the PV-RT power system, ΔF_1 and ΔF_2 represent the frequency change in the first region and the second region, respectively. ΔP_{tie} represents the change of power between areas. ΔP_{L1} and ΔP_{L2} represent the load change in the first and second areas, respectively. The R parameter at the governor input in the second area is the speed regulation coefficient. PV power plant model consists of PV panel, maximum power point tracker, converter, and filter units [5]. The transfer function representing of this model is given below.

$$G_{\mathrm{PV}}(s) = \frac{sb + a}{s^2 + sc + d} \tag{1}$$

The reheat thermal power plant model consists of the governor, turbine, reheater, and generator-load units. The transfer function presentations of these units are given in Table 2.

The error received from the feedback for an area is called area control error (ACE) [51]. ACE_1 and ACE_2 (controller inputs) for the first and second regions are given below, respectively.

$$e_1(t) = \mathrm{ACE}_1 = \Delta P_{\mathrm{tie}} \tag{2}$$

$$e_1(t) = \mathrm{ACE}_2 = B\Delta F_2 - \Delta P_{\mathrm{tie}} \tag{3}$$

where B is the frequency bias parameter. The power change between regions is calculated as follows.

$$\Delta P_{\mathrm{tie}} = \frac{T_{12}}{s}\left[\Delta F_1 - \Delta F_2\right] \tag{4}$$

Table 2 Reheat thermal power plant model units

Governor	Turbine	Reheater	Generator-load (/Power System)
$G_G(s) = \frac{1}{sT_g+1}$	$G_T(s) = \frac{1}{sT_t+1}$	$G_R(s) = \frac{sK_rT_r+1}{sT_r+1}$	$G_P(s) = \frac{K_{ps}}{sT_{ps}+1}$

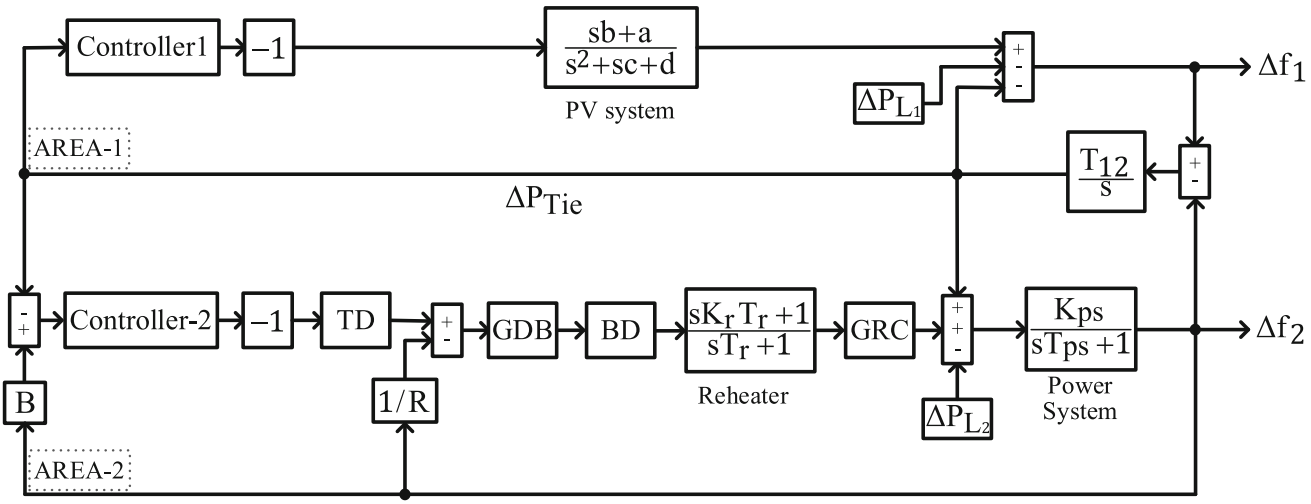


Fig. 2 PV-RT power system with nonlinear effects

where T_{12} is the synchronization constant of the connecting line. The parameters of this power system are given in Appendix 15.

2.2 Nonlinear effects

This section describes the models and properties of nonlinear effects used in the study. PV-RT power system model with the considered nonlinear effects is given in Fig. 2.

The properties of the four different nonlinear blocks in Fig. 2 are given below.

- Governor Dead Band (GDB): In the real power system, it is stated in the literature that GDB can significantly affect the system performance [52]. GDB is defined as the total magnitude of a continuous speed change with no change in the valve position of the turbine [4, 53].
- Generation Rate Constraint (GRC): GRC is a physical constraint that means the practical limit of the rate of change in generation power due to thermodynamic and mechanical constraints in steam turbine systems applications. Due to the nonlinearity of GRC, it has a great impact on power system performance [4].
- Boiler Dynamics (BD): In this study, drum type BD is considered [54]. A boiler is defined as a device designed to produce steam under pressure. In addition, drum-type boilers are also called circulating boilers [55]. The system parameters used in the study are shared in the 15
- Time Delay (TD): TD is presented in physical systems, and it is an important parameter that affects system stability [4]. TD can degrade system performance or even make it unstable [56]. Therefore, it must be taken into account in the controller design. In this study, the TD is chosen as 50 ms as recommended in [57, 58].

The models of the nonlinear blocks mentioned above are given in Fig. 12.

2.3 Cyber-attack

In large-scale power systems, the balance between electricity generation and consumption is based on instantaneous changes in electricity consumption demand. Attackers can attack control centers and communication channels [41]. In this way, the attacker can disrupt the requested load input signals.

This section discusses two different C-A methods for generating a fake load input signal. These attack methods are ResA and RndA. ResA requires system information while RndA does not. In a ResA, the attacker changes the load according to the resonance source, but this change must be within acceptable limits [41]. "Acceptable limits" are such small changes in the load that the attack cannot be detected. By using a resonance source, small but continuous changes in load are targeted. Therefore, large deviations in frequency and rate of change of frequency (RoCoF) are achieved. In power systems, RoCoF protection relays are usually set to trip in the range 0.1−1.0 Hz/s [59]. As a result of the attack, RoCoF relays can be tripped to protect electrical equipment [41]. This can lead to major outages in power systems. This

attack method can be described with 6 steps given below [41].

- The frequency (generally) output of the grid is used as a resonance source. (This step is required for ResA.)
- The fake input is sent to the generator system.
- The generator system checks whether the input is within acceptable limits.
- If the input is within acceptable limits, the generator system is controlled to reach the target power. (If the input is not within acceptable limits, the attack is detected.)
- Generator produces electricity according to fake input.
- The protection relay trips when the RoCoF is out of the acceptable limit.

If the attack is not successful, the resonance source or the attack size can be changed. Then, the steps described above are repeated. The attack entry must not be greater than 0.3 pu; otherwise, an attack is detected [41].

The RndA is very similar to the ResA. An attack with ResA uses the frequency response of the system, while an attack with RndA is random. In other words, the attack model is created without using a resonance source. The mathematical models of ResA and RndA are given in eq. (5) and eq. (6).

$$\Delta P_{L_2} = -0.1.sign\left(\Delta f'_2\right) \tag{5}$$

$$\Delta P_{L_2} = -0.1.sign\left(\sin(\omega t)\right), \omega = 2\pi f, \quad f = 3 \tag{6}$$

In ResA (in eq. (5)), the frequency change in the second region is chosen as the resonance source and the attack is modeled according to this source. In RndA (in eq. (6)), the attack is modeled with a sinusoidal wave. The attack frequency (f) used in RndA can be chosen randomly. In both ResA and RndA, the size of the attack is limited to 0.1 pu. This limitation is sufficient to compare attacks and measure the performance of controllers.

2.4 Fractional and integer order controllers

In this section, fractional calculus definitions are discussed. Also, the structure of the controllers used in the study is introduced.

2.4.1 Fractional Calculus

The TID controller is obtained by adding a fractional order integrator with K_p coefficient instead of the proportional term of a PID controller. Therefore, the TID controller is modeled using fractional calculus. Fractional calculus is modeled with the continuous integral-derivative operator [60]. This operator is given below.

$${}_aD_t^{\alpha} = \begin{cases} \frac{d^{\alpha}}{d}t^{\alpha}, & \Re(\alpha) > 0, \\ 1, & \Re(\alpha) = 0, \\ \int_a^t (d\tau)^{-\alpha}, & \Re(\alpha) < 0, \end{cases} \tag{7}$$

where a and t are the limits of the operation, α is the order of operation. The continuous integral-derivative operator can be easily used in the Laplace domain with the Oustaloup approximation method. This method is often used because it performs well in control studies. The equation of the Oustaloup approximation method is given in eq. (8).

$$s^{\alpha} \approx \omega_h^{\alpha} \prod_{k=-N}^{N} \frac{s+\omega_z}{s+\omega_p}, for\ 0 < \alpha < 1 \tag{8}$$

where N is the number of pole-zero pairs [61] and using this, the order of the Oustaloup filter can be determined as $(2N + 1)$. Also, ω_p and ω_z are poles and zeros, respectively. With the development of the Oustaloup approximation method, the refined Oustaloup filter approximation method has been introduced. This advanced method has high accuracy over a wide frequency range [62]. The mathematical representation of the refined Oustaloup filter method is given in eq. (10) [63].

$$s^{\alpha} \approx \left(\frac{d}{b}\omega_h\right)^{\alpha} \frac{ds^2 + b\omega_h s}{d(1-\alpha)s^2 + b\omega_h s + d\alpha} \prod_{k=-N}^{N} \frac{s+\omega_z}{s+\omega_p}, for\ 0 < \alpha < 1 \tag{9}$$

where b and d coefficients are chosen as 10 and 9, respectively [64]. In both the Oustaloup approximation and the refined Oustaloup filter approximation methods, poles, and zeros are calculated as follows.

$$\omega_p = \omega_b\left(\frac{\omega_h}{\omega_b}\right)^{\frac{k+N+0.5(1+\alpha)}{2N+1}}, \ \omega_z = \omega_b\left(\frac{\omega_h}{\omega_b}\right)^{\frac{k+N+0.5(1-\alpha)}{2N+1}} \tag{10}$$

where ω_h and ω_b are the frequency band upper and lower bounds, respectively.

2.4.2 PID/TID/PI-PD/TI-TD controllers

The transfer function of a PID controller is shown below.

$$\text{Controller}_{\text{PID}} = K_p + sK_d + \frac{1}{s}K_i \tag{11}$$

Using fractional order mathematics, the TID controller can be written in the Laplace domain as follows.

$$\text{Controller}_{\text{TID}} = \frac{1}{s^{1/n}} K_T + sK_d + \frac{1}{s} K_i, 1/n \ = \alpha = \lambda \tag{12}$$

The PI-PD controller structure is obtained by cascading PI and PD controllers. The transfer function of the PI-PD controller is given below.

$$\begin{aligned} \text{Controller}_{\text{PI-PD}} &= \left(K_{p_1} + \frac{1}{s} K_i\right)\left(K_{p2} + sK_d\right) \\ &= K_{p_1} K_{p2} + sK_{p_1} K_d + \frac{1}{s} K_i K_{p2} + K_i K_d \end{aligned} \tag{13}$$

The TI-TD controller is similar to the PI-PD controller. The difference between the two controllers is the T parameter. The transfer function of the TI-TD controller is given below.

$$\begin{aligned} \text{Controller}_{\text{TI-TD}} &= \left(\frac{1}{s^{\lambda_1}} K_{T_1} + \frac{1}{s} K_i\right)\left(\frac{1}{s^{\lambda_2}} K_{T_2} + sK_d\right) \\ &= \frac{1}{s^{\lambda_1+\lambda_2}} K_{T_1} K_{T_2} + \frac{1}{s^{\lambda_1-1}} K_{T_1} K_d \\ &\quad + \frac{1}{s^{\lambda_2+1}} K_i K_{T_2} + K_i K_d \end{aligned} \tag{14}$$

2.5 Optimization process

In this section, MA which has been used as an optimization algorithm in the study is explained and the objective function of the system is defined.

2.5.1 Mayfly algorithm

MA is one of the recently proposed metaheuristic algorithms [42]. Mayfly (Ephemeroptera) is an amphiprotic insect that has a short lifetime and appears in mainly May in a year [65, 66]. Mayflies have a metamorphic life cycle. They pass their nymph life periods in the water until they grow up and being adults. In that metaheuristic algorithm which is inspired by the social behaviors of mayflies, it is supposed that the mayflies are adults after hatching from the egg and the fittest mayflies survive regardless of how long they live [42]. Elements of MA can be expressed as below:

1. Movements of Male Mayflies Male mayflies in a swarm adjust their positions based on their experiences and the positions of their neighboring individuals while performing nuptial dances above water. The male mayfly position is updated as in eq. (15).

$$x_i^{t+1} = x_i^t + v_i^{t+1} \tag{15}$$

where x_i^t defines present position of the i th male mayfly at the time step t, x_i^{t+1} is the updated position of i th male mayfly and v_i^{t+1} is the velocity of the i th male mayfly. The velocity of the i th male mayfly is modeled as in eq. (16).

$$\begin{aligned} v_{ij}^{t+1} &= v_{ij}^t + \psi_1 e^{-\beta\lambda_p^2}\left(p\text{best}_{\text{ij}} - x_{ij}^t\right) \\ &\quad + \psi_2 e^{-\beta\lambda_g^2}\left(g\text{best}_{\text{j}} - x_{ij}^t\right) \end{aligned} \tag{16}$$

v_{ij}^t is the velocity of the i th male mayfly at the time step t in dimension $j = 1, ..., n$. ψ_1 and ψ_2 are positive attraction constants applied to scale the contribution of the social and cognitive components, respectively. On the other hand, $pbest_i$ denotes the best position of the i th male mayfly had ever visited. Given the minimization problems, the personal best position $p\text{best}_{\text{ij}}$ at the time step $t + 1$ is calculated as;

$$p\text{best}_{\text{i}} = \begin{cases} x_i^{t+1}, if\ f(x_i^{t+1}) < f(p\text{best}_{\text{i}}) \\ \text{is kept the same, otherwise} \end{cases} \tag{17}$$

Lastly, β represents a visibility coefficient that limits the visibility of a mayfly to the other mayflies, λ_p is the Cartesian distance between x_i and $p\text{best}_{\text{i}}$, λ_g is the Cartesian distance between x_i and $gbest$. These are calculated as below;

$$\|x_i - \chi_i\| = \sqrt{\sum_{j=1}^{n} \left(x_{ij} - \chi_{ij}\right)^2} \tag{18}$$

x_{ij} denotes j^{th} element of the i^{th} male mayfly and χ_i corresponds to $pbest_i$ or $gbest$. While male mayflies dance up to down, the best mayflies have to update their velocities as defined mathematically in eq. (19);

$$v_{ij}^{t+1} = v_{ij}^t + d * r \tag{19}$$

In eq. (19), d denotes nuptial dance coefficient and r is a random value $\in [-1,\ 1]$ [42].

2. Movements of Female Mayflies Female mayflies exhibit distinct movements from males. They are attracted by males in order to fly toward the swarm to mate. The attraction process is modeled as a deterministic process that involves velocity calculation of each male and female mayfly by using the fitness function [42, 67, 68]. Considering the y_i^t is the position of the i^{th} female mayfly at time step t, next position of the i^{th} female mayfly at

time step $t+1$ by adding a velocity v_i^{t+1} can be defined as follows;

$$y_i^{t+1} = y_i^t + v_i^{t+1} \tag{20}$$

As a result velocities of the females can be expressed mathematically as below;

$$v_{ij}^{t+1} = \begin{cases} v_{ij}^t + \psi_2 e^{-\beta\lambda_{mf}^2}\left(x_{ij}^t - y_{ij}^t\right), if\ f(y_i) > f(x_i) \\ v_{ij}^t + fl * r, if\ f(y_i) \le f(x_i) \end{cases} \tag{21}$$

where v_{ij}^{t+1} is the velocity of the i^{th} female mayfly at the time step t in dimension $j = 1, ..., n$, y_{ij}^t is the position of the i^{th} female mayfly in j^{th} dimension at time step t, ψ_2 is positive attraction constants applied to scale the contribution of the social and cognitive component, β is visibility coefficient, λ_{mf} is the Cartesian distance between male and female mayflies. Finally, fl is used when a female is not attracted by a male, denotes the random walk coefficient, r is a random value $\in [-1, 1]$ [42].

3. Mating the Mayflies Mayflies employ a crossover operator during their mating process. For producing two offspring, the highest-fitness female pairs with the highest-fitness male, while the second-best female pairs with the second-best male, and so forth. The results of the crossover are two offspring which are produced as follows:

$$\text{offspring}_1 = L * \text{male} + (1 - L) * \text{female} \tag{22}$$

$$\text{offspring}_2 = L * \text{female} + (1 - L) * \text{male} \tag{23}$$

where $male$ represents male parent, $female$ represents female parent, L is the predefined random number in a certain range. Initial velocities of the offspring are set to be zero [42, 67, 68]. The pseudo-code of MA is shown below;

Algorithm 1 Mayfly [42]

Objective Function $f(x)$, $x = (x_1, \ldots, x_d)^T$
Initialize: *The population of male Mayfly* $x_i (i = 1, 2, \ldots, N)$ *and velocities* v_{mi}
Initialize: *The population of female Mayfly* $y_i (i = 1, 2, \ldots, M)$ *and velocities* v_{fi}
Evaluate Solutions
Obtain gbests by using eq. (24)
do
  Update velocities and solutions of all mayflies
  Evaluate Solutions
  Rank the mayflies
  Mate the mayflies
  Evaluate offsprings
  Separate offspring to all mayflies randomly
  Change the worst solutions with the best ones
  Update pbest and gbest
while *stopping criteria are not met*
Postprocess results and visualization

2.5.2 Objective function

In this study, the integral of the time-weighted absolute error (ITAE) is used as the objective function. The mathematical expression of the objective function used is given in eq. (24).

$$\text{ITAE} = \int_0^{t_{\text{sim}}} t(|\Delta F_1| + |\Delta F_2| + |\Delta P_{\text{tie}}|)\mathrm{d}t \tag{24}$$

where ΔF_1 and ΔF_2 are the frequency change in the first and second area, respectively, and ΔP_{tie} is the power change in the tie line.

2.5.3 Constraints for the optimization problem

In an optimization problem, variables typically have constraints. When dealing with an optimization problem, it is essential to ensure that the given constraints are not violated. In this regard, the lower and upper bounds of the variables are determined in Table 3 for the considered optimization problem. These constraints are used in both linear and nonlinear systems. In nonlinear systems, GRC is additionally used as a constraint. As mentioned before, GRC limits the rate of change in power generation [4]. The lower and upper limits of the saturation block in GRC are ± 0.0017 p.u./s [53].

3 Simulation studies and results

In this section, the control of linear (without GDB-GRC-BD-TD) and nonlinear (with GDB-GRC-BD-TD) PV-RT power systems is discussed. The above-mentioned GDB, GRC, BD, and TD are used for the nonlinear modeling of the LFC system. The parameters of four different controllers (PID/TID/PI-PD/TI-TD) for both linear and nonlinear system models are optimized with MA. Nonlinear system models are considered for two different cases. These cases are system models including GDB-GRC and GDB-GRC-BD-TD nonlinear effects. The first (GDB-GRC) of these two nonlinear models is often considered together in the literature and is chosen because the GRC effect is dominant. The other one (GDB-GRC-BD-TD) is chosen because it includes all nonlinear effects.

Optimization of controllers for linear and nonlinear system models is discussed in the sub-title of time domain analysis (TDA). In this section, robustness and RLC analyses are also performed for the linear system model.

Table 3 Controller structures and parameter ranges used in the first and second areas

Evaluation	$K_{p1}(/K_p)$	K_{p2}	K_{t1}/K_t	K_{t2}	K_i	K_d	$\lambda_1(/\lambda)$	λ_2
PID	0.001−2	–	–	–	0.001−2	0.001−2	–	–
TID	–	–	0.001−2	–	0.001−2	0.001−2	0.1−1	–
PI − PD	0.001−2	0.001−2	–	–	0.001−2	0.001−2	–	–
TI − TD	–	–	0.001−2	0.001−2	0.001−2	0.001−2	0.1−1	0.1−1

Table 4 Literature comparison for ITAE values

Reference No	[24]		[46]			[5]		
Control Type	PI	PI	PI	PID	PID	PI	PID	PIDF
Algorithm	GA	FA	SFLA	SFLA	gSLFA-PS	WOA	MWOA	MWOA
ITAE	12.124	7.4259	4.5432	2.1125	1.8142	4.1211	1.5602	1.4841
Reference No	[49]				This Study			
Control Type	PID	PID	TID		PID	TID	PI-PD	TI-TD
Algorithm	GWO-CS	MGWO-CS	MGWO-CS		MA	MA	MA	MA
ITAE	1.1160	1.0520	0.9203		0.7577	0.5979	0.3379	0.2625

3.1 Time domain analysis

The parameter range for the controller must be determined in order to obtain parameter values in the optimization process. The parameter range should be selected according to the studies in the literature [5, 24, 46, 69]. Otherwise, it would not be fair to compare the study with the studies in the literature. When the studies in the literature are examined, SLP is taken as 10% (Area-2) for the linear system [5, 24, 46, 55, 69] and 1% (Area-2) for the nonlinear system [4, 27, 55, 70] during the optimization process. Therefore, SLP is taken as 10% (Area-2) for the linear system and 1% (Area-2) for the nonlinear system in this study.

In this study, controllers in two areas are considered separately for the PV-RT power system. Controller structures and parameter ranges used in the first and second areas are given in Table 3.

3.1.1 PV-RT power system

The parameter and ITAE values obtained as a result of the optimization process are given in Table 4 for SLP 10%. In addition, ITAE values of the studies conducted in the literature using the same system parameters, SLP ratio/region, and controller parameter range are given in [5, 24, 46, 49]. When the results of the studies in the literature are examined, it is seen in Table 4 that they obtained higher ITAE values even for the PID controller. The lower ITAE value obtained with the PID controller in this study shows the success of MA. When ITAE values are examined, cascade controllers (PI-PD/TI-TD) give better results for this system than other controllers (PID/TID). For this system, the TID controller (0.5979) gives better results than the PID controller (0.7577) and TI-TD (0.2625) controller gives better results than PI-PD (0.3379) controller.

In Table 5, the controller used in the first area (Area-1) represents the expression A1, and the controller used in the second area (Area-2) represents the expression A2.

The transient responses of all controllers are given in Table 6 where the best results are shown in bold.

The values in Table 6 as a result of the transient response can be summarized as follows.

- For the frequency change in the first area (Δ_{F1}) and power change in the tie-line ($\Delta_{P\text{tie}}$), the TI-TD controller provides the best T_s. On the other hand, for the frequency change in the second area (Δ_{F2}), the PI-PD controller achieves the best result at settling time.
- When the results of the undershoot and overshoot are examined, it is seen that the controllers give similar results to the settling time. The TI-TD controller gives great results compared to other controllers for overshoot and undershoot in frequency change of the first area and power change in the tie-line.
- Except for the overshoot result in the second region, the TI-TD controller shows superior performance for this system. In addition, the performance of the PI-PD controller for this system is better than the PID and TID controllers.

[5, 46, 49] accepted [24] as a reference. For this reason, [24] is taken as a reference in this study. Figure 3 compares the results of this study with the reference study. In addition to the ITAE values, it is seen in Fig. 3 that the results obtained in this study show superior performance compared to the reference study.

Table 5 Optimum controller parameters and corresponding ITAE values

Contr. type	ITAE	Gain parameters						Integral param.	
		K_{p1}	K_{p2}	K_{t1}	K_{t2}	K_i	K_d	λ_1	λ_2
PID^{A1}	0.7577	0.0406	–	–	–	0.0129	0.0653	–	–
PID^{A2}		2	–	–	–	2	0.5621	–	–
TID^{A1}	0.5979	–	–	0.0551	-	0.0153	0.1336	0.1	–
TID^{A2}		–	–	2	–	2	0.9202	0.3061	–
PI – PD^{A1}	0.3379	2	0.0112	–	–	1.0461	0.0125	–	–
PI – PD^{A2}		2	2	–	–	2	0.5606	–	–
TI – TD^{A1}	0.2625	–	–	0.0294	0.9247	0.0020	2	0.1	0.4515
TI – TD		–	–	1.9998	2	2	1.5041	0.4204	0.1

Table 6 Transient response performances of the controllers

Controller	Settling Time (0.2%)			Undershoot (p.u)			Overshoot (p.u)		
	Δ_{F1}	Δ_{F2}	$\Delta_{P\text{tie}}$	Δ_{F1}	Δ_{F2}	$\Delta_{P\text{tie}}$	Δ_{F1}	Δ_{F2}	$\Delta_{P\text{tie}}$
PID	8.76	5.97	11.66	−0.0494	−0.1290	−0.0057	0.0024	0.0164	0.0303
TID	3.1	5.31	10.26	−0.0581	−0.1157	−0.0042	0.0031	0.0269	0.0269
PI – PD	3.79	**1**	8.64	−0.0202	**−0.0859**	−0.0033	0.0011	**0.0024**	0.0155
TI – TD	**3**	3.38	**6.58**	**−0.0187**	−0.0893	**−0.0022**	**7.2e−04**	0.0278	**0.0129**

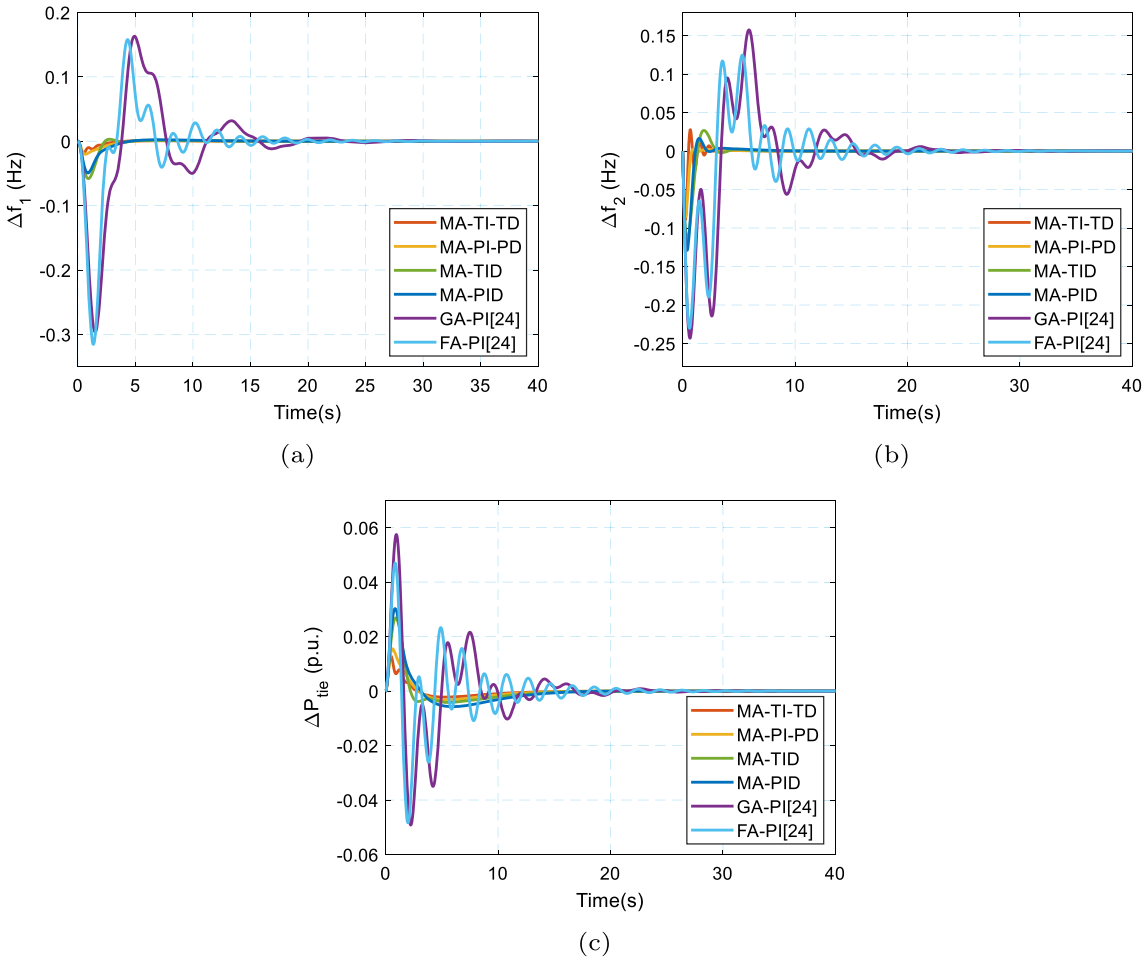


Fig. 3 Transient responses of the controllers. **a** Δ_{F1}, **b** Δ_{F2}, **c** Δ_{Ptie}

Table 7 Optimum controller parameters and corresponding ITAE values with GDB-GRC

Contr. Type	ITAE	Gain Parameters						Integral Param.	
		K_{p1}	K_{p2}	K_{t1}	K_{t2}	K_i	K_d	λ_1	λ_2
PID^{A1}	0.4325	0.0279	–	–	–	0.001	0.1285	–	–
PID^{A2}		1.1159	–	–	–	0.19	1.2618	–	–
TID^{A1}	0.4612	–	–	0.0189	–	0.001	0.1325	0.1	–
PID^{A2}		–	–	0.759	–	0.194	1.0655	0.1001	–
$PI-PD^{A1}$	0.2893	0.9885	0.0112	–	–	0.001	0.0393	–	–
$PI-PD^{A2}$		0.3944	0.2157	–	–	0.926	1.8723	–	–
$TI-TD^{A1}$	0.2985	–	–	0.0125	0.001	0.0048	1.6493	0.1	0.1
$TI-TD^{A2}$		–	–	1.0476	1.1354	0.1115	0.8460	0.1	0.1

Table 8 Transient response parameters of the controllers with GDB-GRC

Controller	Settling Time (0.04%)			Undershoot (p.u)			Overshoot (p.u)		
	Δ_{F1}	Δ_{F2}	Δ_{Ptie}	Δ_{F1}	Δ_{F2}	Δ_{Ptie}	Δ_{F1}	Δ_{F2}	Δ_{Ptie}
PID	6.21	7.61	7.14	−0.0226	−0.0339	–3.6e−04	4.0e−05	**0.0012**	**0.0116**
TID	**6.06**	7.53	23.17	−0.0223	−0.0339	−4.5e−04	**3.5e−05**	0.0020	0.0117
PI-PD	6.18	**6.76**	6.33	−0.0170	−0.0326	**−5.4e−06**	1.5e−04	0.0080	0.0130
TI-TD	6.29	6.77	**6.30**	**−0.0158**	**−0.0323**	–7.8e−06	8.5e−05	0.0095	0.0134

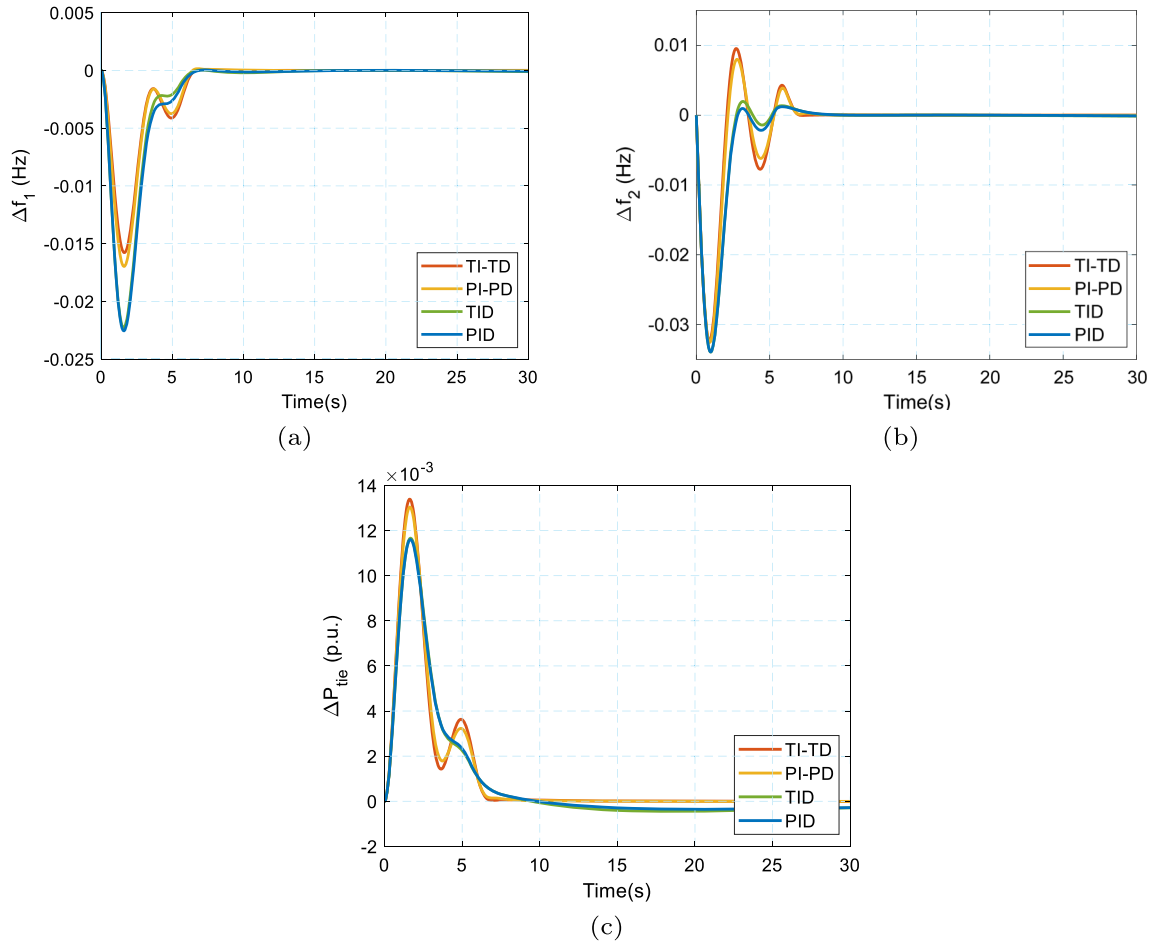


Fig. 4 Dynamic responses of the controllers with GDB and GRC. **a** Δ_{F1}, **b** Δ_{F2}, **c** Δ_{Ptie}

Table 9 Optimum controller parameters and corresponding ITAE values with GDB-GRC-BD-TD

Contr. Type	ITAE	Gain Parameters						Integral Param.	
		K_{p1}	K_{p2}	K_{t1}	K_{t2}	K_i	K_d	λ_1	λ_2
PID^{A1}	0.4635	0.0277	–	–	–	0.001	0.1306	–	–
PID^{A2}		1.0391	–	–	–	0.2181	1.1122	–	–
TID^{A1}	0.4946	–	–	0.0206	–	0.001	0.1337	0.1	–
TID^{A2}		–	–	0.6885	–	0.2212	0.6832	0.1	–
$PI-PD^{A1}$	0.2986	2	0.0039	–	–	0.001	0.0303	–	–
$PI-PD^{A2}$		0.6282	0.2122	–	–	1.0814	1.3763	–	–
$TI-TD^{A1}$	0.3018	–	–	1.0243	0.001	0.001	0.0296	0.1	0.1
$TI-TD^{A2}$		–	–	0.601	1.9733	0.078	1.4704	0.1	0.1002

Table 10 Transient response parameters of the controllers with GDB-GRC-BD-TD

Controller	Settling Time (0.04%)			Undershoot (p.u)			Overshoot (p.u)		
	Δ_{F1}	Δ_{F2}	Δ_{Ptie}	Δ_{F1}	Δ_{F2}	Δ_{Ptie}	Δ_{F1}	Δ_{F2}	Δ_{Ptie}
PID	6.24	7.47	7.38	−0.0229	−0.0343	−3.6e−04	**4.9e−06**	**0.0013**	**0.0117**
TID	6.06	7.12	21.84	−0.0226	−0.0343	−4.5e−04	9.8e−06	0.0017	0.0118
PI-PD	**6.04**	7.39	7.48	−0.0182	−0.0332	**−3.1e−06**	2.1e−04	0.0070	0.0129
TI-TD	6.11	**6.74**	**6.48**	**−0.0161**	**−0.0327**	−3.9e−06	2.5e−04	0.0097	0.0135

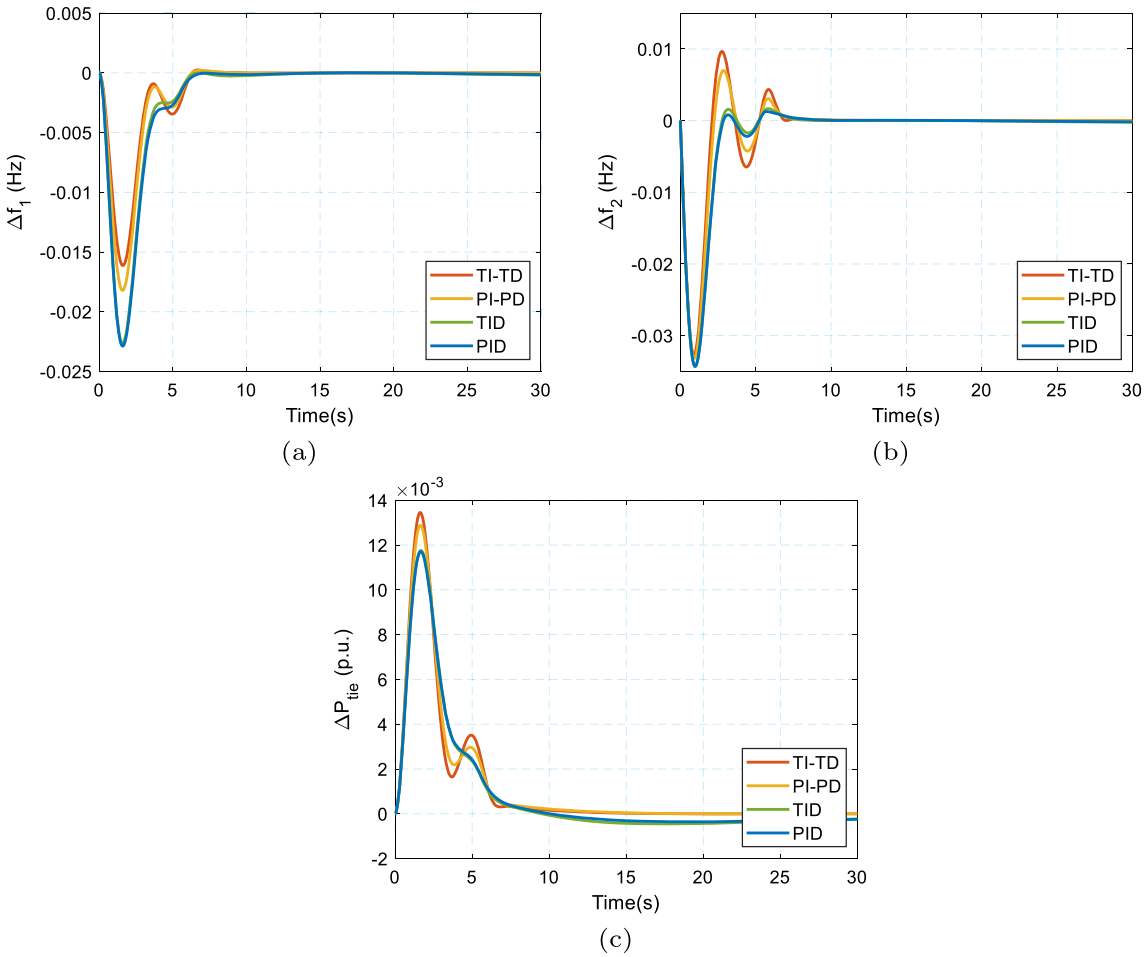


Fig. 5 Dynamic responses of the controllers with GDB, GRC, BD, and TD. **a** Δ_{F1}, **b** Δ_{F2}, **c** Δ_{Ptie}

Table 11 Robustness Analysis Results

Par.	Rate of Change	Settling Time (0.2%)			Undershoot (p.u)			Overshoot (p.u)		
		Δ_{F1}	Δ_{F2}	Δ_{Ptie}	Δ_{F1}	Δ_{F2}	Δ_{Ptie}	Δ_{F1}	Δ_{F2}	Δ_{Ptie}
τ_G	+75	5.78	10.73	7.7	−0.023	−0.1034	−0.0037	0.0027	0.0644	0.0158
	+50	3.35	6.29	6.6	−0.0216	−0.0991	−0.0027	0.0012	0.0526	0.0149
	-50	2.97	3.25	6.61	−0.0161	−0.077	−0.0022	0.0007	0.0047	0.011
	-75	2.99	3.26	6.62	−0.0151	−0.0699	−0.0022	0.0007	0.0025	0.0104
τ_T	+75	3.01	5.86	6.79	−0.0271	−0.1106	−0.0029	0.0014	0.0672	0.0186
	+50	2.85	5.03	6.49	−0.0245	−0.1043	−0.0024	0.0009	0.0549	0.0168
	-50	3.09	3.27	6.64	−0.013	−0.069	−0.0022	0.0007	0.0026	0.0087
	-75	3.17	3.32	6.68	−0.0125	−0.0543	−0.0022	0.0007	0.0024	0.0084
τ_{12}	+75	2.34	4	6.41	−0.0269	−0.0862	−0.0025	0.0009	0.0335	0.0186
	+50	2.42	4	6.45	−0.0245	−0.0871	−0.0024	0.0008	0.0336	0.0169
	-50	3.74	4.5	2.61	−0.0111	−0.0917	−0.0018	0.0005	0.0183	0.0076
	-75	4.88	5.81	2.93	−0.0065	−0.0931	−0.0012	0.0003	0.0114	0.0042
B	+75	2.83	3.72	2.17	−0.0114	−0.0697	−0.0017	0.0008	0.0248	0.0079
	+50	2.73	3.39	2.03	−0.0131	−0.0747	−0.0018	0.0008	0.0247	0.0091
	-50	3.26	4.58	7.59	−0.0317	−0.1185	−0.0029	0.0004	0.0524	0.0217
	-75	5.65	11.37	8.07	−0.0466	−0.1491	−0.0071	0.0058	0.1026	0.0317
R	+75	2.96	3.41	6.58	−0.019	−0.0897	−0.0022	0.0007	0.0272	0.0131
	+50	2.97	3.4	6.58	−0.0189	−0.0896	−0.0022	0.0007	0.0273	0.013
	-50	3.05	4.02	6.6	−0.0182	−0.0882	−0.0022	0.0007	0.0294	0.0125
	-75	3.07	3.96	6.59	−0.0172	−0.0863	−0.0022	0.0007	0.0324	0.0118

3.1.2 PV-RT power system with GDB-GRC

In this section, the nonlinear effect of GDB and GRC together is examined for the PV-RT power system. The optimum controller parameters with corresponding ITAE values obtained for this system are given in Table 7.

When the results in Table 5 are compared to the results in Table 8, it is seen that the ITAE performances of the controllers with similar structures (PID/TID, PI-PD/TI-TD) are close to each other. The ITAE result obtained for the PI-PD controller is almost the same as for the TI-TD controller. This situation is also seen in the results given in Table 7. For transient response, the best results are shown in bold in Table 8.

The results obtained in Table 8 can be summarized as follows.

- In terms of settling time, it is seen that cascade controllers give better results than others for a frequency change of the second area and power change of the tie-line. However, the results of all controllers are close to each other in the frequency change of the first area.
- When cascade controllers are used in the system, it is seen that the undershoot value for frequency and power change decreases. However, PID and TID controllers are more successful than cascade controllers in terms of overshoot.

Figure 4 shows transient responses of the controllers with GDB and GRC.

3.1.3 PV-RT power system with GDB-GRC-BD-TD

The nonlinear effect of TD is analyzed in this section. The results of the optimization process for the PV-RT power system with GDB-GRC-BD-TD are given in Table 9.

ITAE values increased with the addition of BD and TD to the previous nonlinear effects (GDB-GRC). Transient response for this system is given in Table 10, and the best results are marked in bold.

The results in this section are close to the results of the previous analysis (with GDB-GRC-BD-TD). On the other hand, the results are slightly worse in terms of transient response than the previous analysis. Figure 5 depicts transient responses for all controllers under the considered nonlinear effects.

3.2 Robustness analysis

Power system parameters may change due to external factors. Stability in the power system should be maintained against changes in system parameters. For this reason, the controller used in the system should perform successfully in terms of stability. In this section, robustness analysis is discussed for

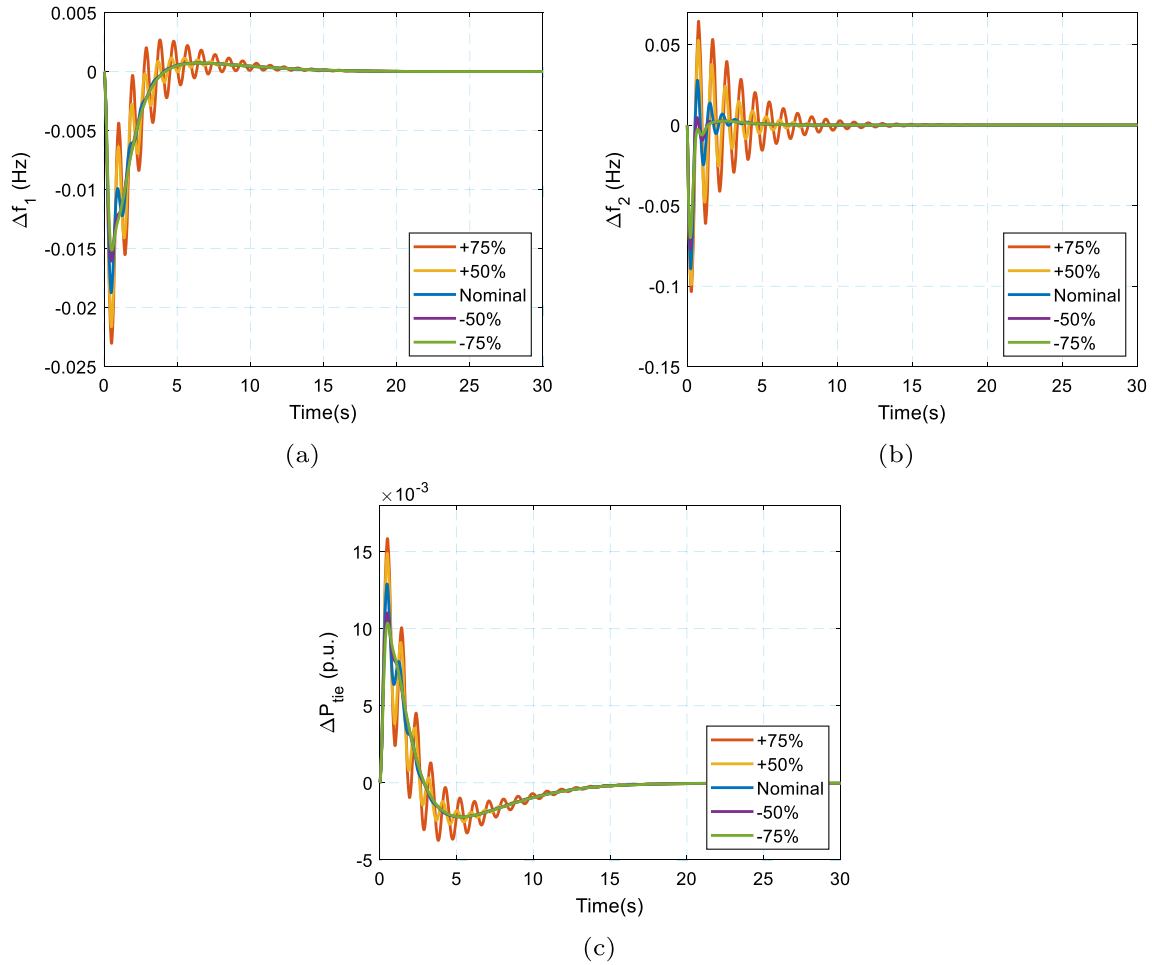


Fig. 6 Sensitivity analysis of the TI-TD controlled linear power system with τ_G variations. **a** Frequency deviation in area-1 **b** Frequency deviation in area-2 **c** Δ_{Ptie}

Table 12 The load change duration and magnitude applied to the system

Time (second)	0–20	20–40	40–60	60–80	80–100
Load Change (p.u.)	0.5	0.75	0.5	0.2	0

linear (without GDB, GRC, BD, TD) PV-RT power systems. For this reason, the SLP value of the system is chosen as 10% for the second area. The TI-TD controller which exhibits the most successful performance for this system is used as the controller in the system. Robustness analysis is performed by changing the τ_G, τ_T, τ_{12}, B and R constants of the system. These changes are selected as -75%, -50%, $+50\%$, $+75\%$. System transient response results are given in Table 11.

In the robustness analysis, the results of five (τ_G, τ_T, τ_{12}, B, R) different system parameters are examined. For this reason, only the transient response for the changes in τ_G is given in Fig. 6.

Robustness Analysis results can be summarized as follows.

- As τ_G increases, the deviations increased for both overshoot and undershoot. In addition, the settling time for frequency changes in the first and second areas also increases with the τ_G.
- As τ_T increases, the deviations increased for both overshoot and undershoot. The increase in the τ_T increases the settling time in the frequency change of the second area. The increase in the τ_T reduces the settling time in the frequency change of the first area.
- As the τ_{12} decreases, the settling time in frequency change increases.
- As the frequency B decreases, the deviations increase for both overshoot and undershoot. However, the change in the frequency B has not a remarkable impact on the overshoot in the first area. The decrease in the bias factor increases the settling time in frequency and power change.
- As the R decreases, the frequency change settling time in the second area increases. In addition, the same effect occurs very little in the frequency change of the first area.

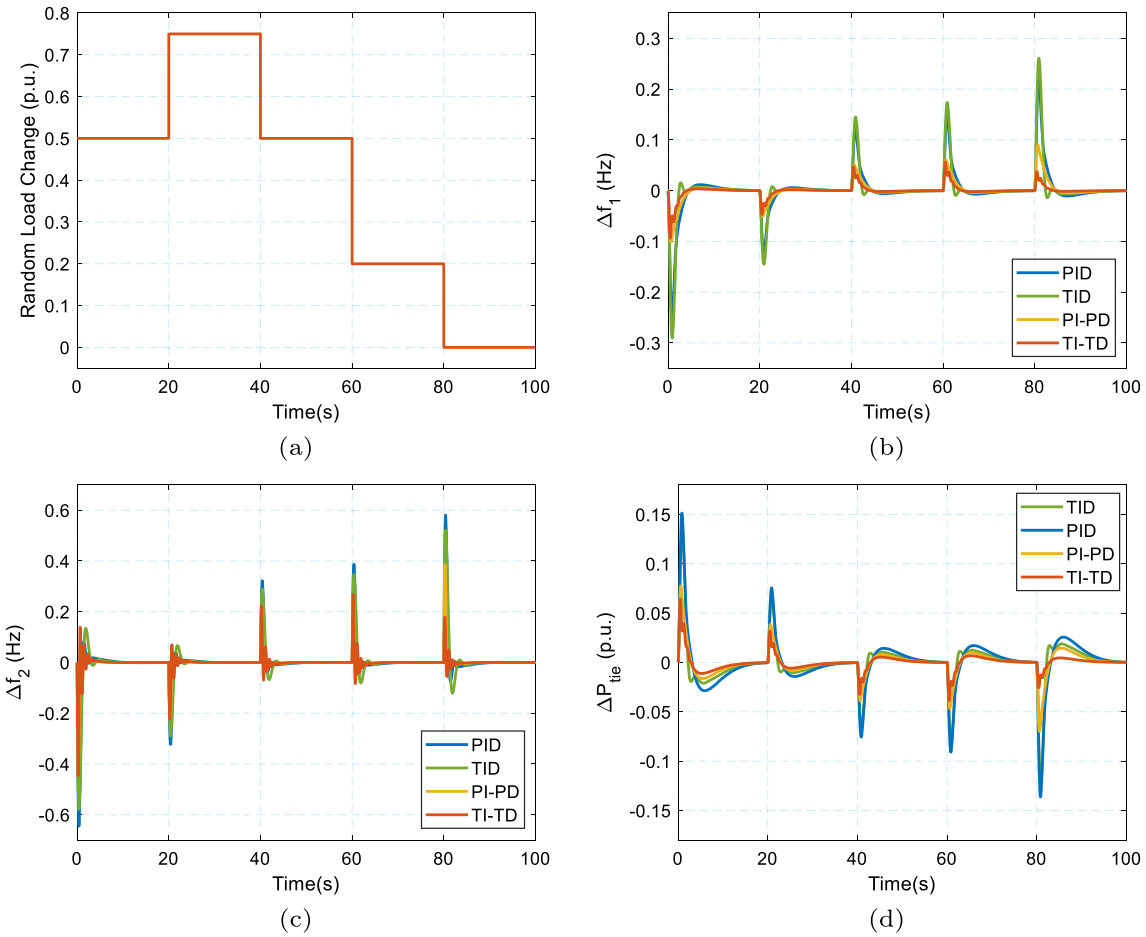


Fig. 7 **a** RLC for PV-RT power system **b** Δ_{F1}, **c** Δ_{F2}, (d) Δ_{Ptie}

The change in R has little effect on overshoot and undershoot.

3.3 Random load change analysis

Load changes are seen commonly in power systems. The power system must be stable under load changes. Therefore, the load change must be analyzed in order to investigate the transient response of the power system.

In this section, RLC analysis considering the studied four controller types is discussed for linear PV-RT power system. The RLC in the system is carried out for the second area. The applied load change pattern to the system is shown in Fig. 7(a).

In Table 12, the load change duration and magnitude applied to the system are given.

The transient response resulting from the RLC analysis is given in Fig. 7.

RLC Analysis results can be commented on as follows.

- The TI-TD controller shows superior performance compared to other controllers. In terms of system stability, the second-best performance is shown by the PI-PD controller.
- The PID controller performed better than the TID controller for the frequency change of the first area. In the second area, the TID controller performed better than the PID controller. The two controllers showed similar results in the power change in the tie-line.

3.4 Cyber-attack in PV-RT power system

In this section, two different C-A methods are discussed. The first of these methods is the resonance attack, which can lead to abnormal frequencies in the power system. As a second method, a random attack is applied to the power system.

3.4.1 Resonance attack

In this attack method, the power load is changed by selecting the RoCoF source signal. Since four different controllers are

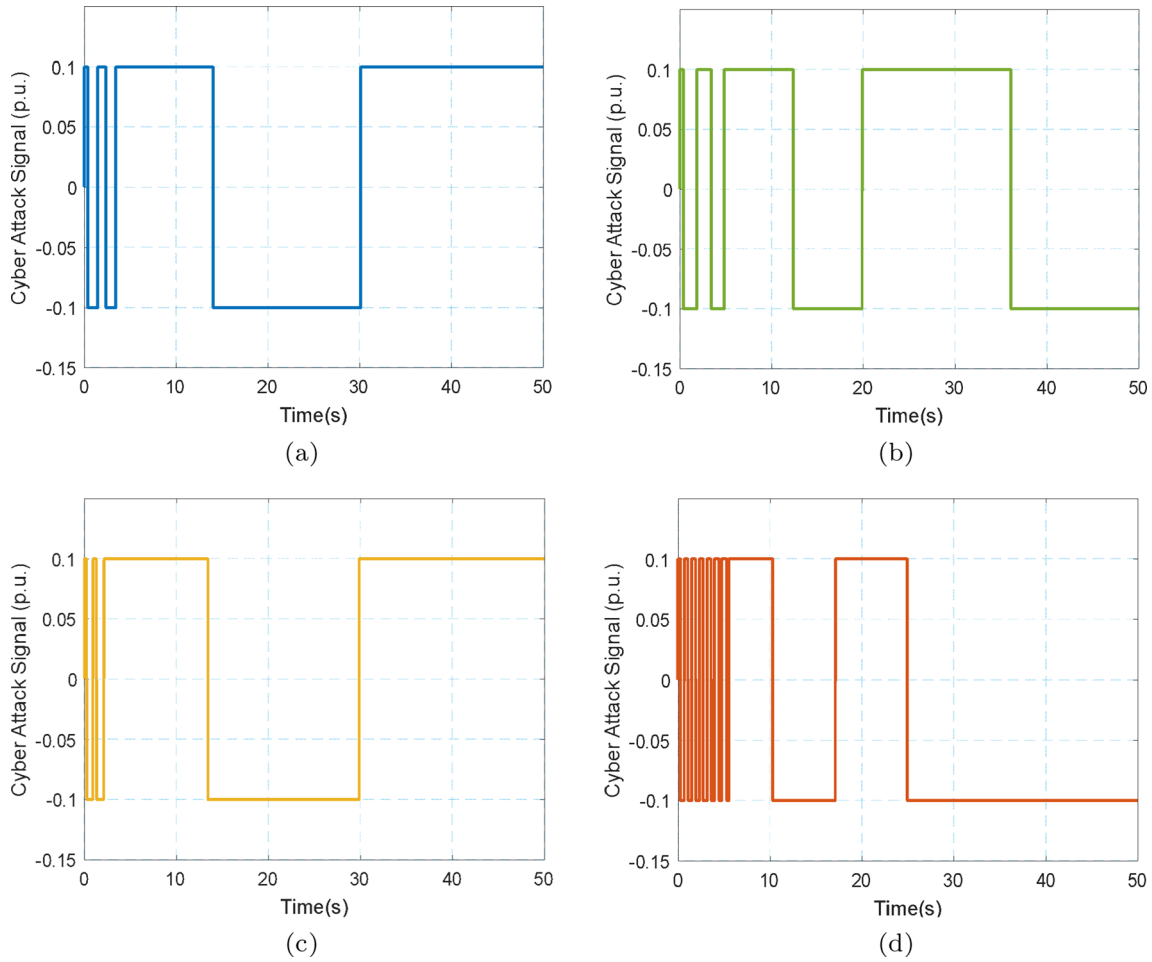


Fig. 8 The C-A signals created for resonance attack method. **a** PID, **b** TID, **c** PI-PD, **d** TI-TD

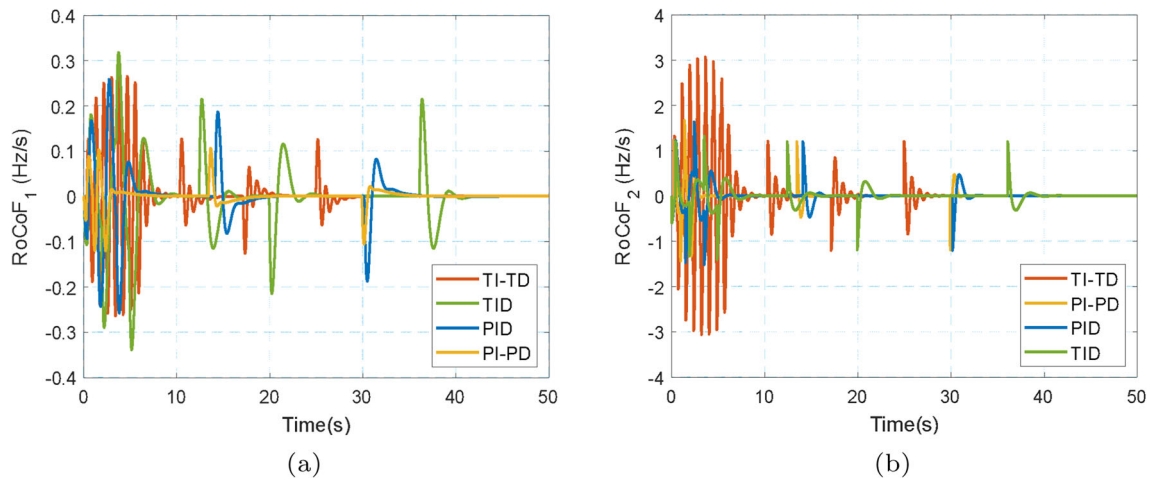


Fig. 9 RoCoF Results of the **a** Area-1, **b** Area-2

used in the study, the response of the power system to the same load change is different. For this reason, a unique resonance attack is created for each system (different controllers). C-A (resonance attack) signals created for each system with different controllers are given in Fig. 8.

The RoCoF of the areas should be examined to correctly interpret the deviations experienced in the system in C-As.

Table 13 Controller performance for ResA

ResA	TI-TD		PI-PD		TID		PID	
	Area 1	Area 2	Area 1	Area 2	Area 1	Area 2	Area 1	Area 2
RoCoF (Hz/s) for 0.1 p.u	0.2668	3.0693	0.1059	1.6711	0.3182	1.3228	0.2586	1.6291
Max. attack mag. (p.u.)	0.032		0.059		0.075		0.061	

The result of this examination is very important. This result gives us information about whether the affected areas should be separated from the power system. The RoCoF results of the areas are given in Fig. 9

If the maximum limit for RoCof relays is accepted as 1.0 Hz/s (generally between 0.1−1.0 Hz/s), RoCoF values in the first area are within an acceptable range, while RoCoF values in the second area are quite high. This means that the second area must be separated from the power system of the field.

The maximum values of RoCoF occurring in the areas for different controllers are given in Table 13. The magnitude of this attack is 0.1 p.u., as previously mentioned. Also, the maximum attack magnitude that the controllers can withstand this type of attack is also given in this table.

According to the attack results (for attack magnitude 0.1 p.u.), in the second region, all attacks are successful as the upper limit of 1.0 Hz/s is exceeded. The maximum attack magnitudes that can be applied to the controllers for the upper limit of 1 Hz/s are also given in Table 13. When the controller performances for the attack magnitudes are analyzed, TID (0.075 p.u.) is the most successful controller, while TI-TD (0.032 p.u.) is the least successful for this type of attack.

3.4.2 Random attack

This attack method models a load change at any frequency value. Thus, a random attack is made on the system without any information. In this section, C-A (random attack) model applied to the power system is given in Fig. 10.

Table 14 shows the controller performances for RndA.

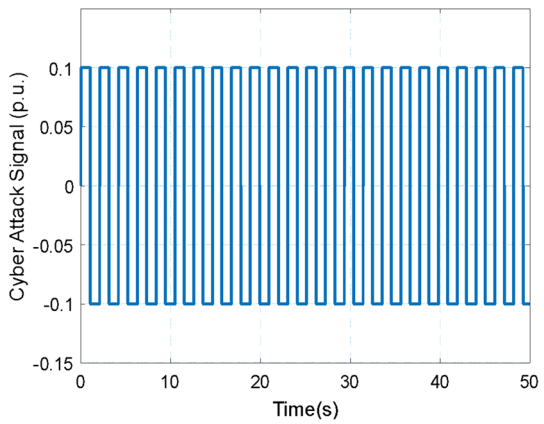


Fig. 10 Random attack signal model applied to the power system

While RoCoF values remained within acceptable limits (for attack magnitude 0.1 p.u.) in the first area, the reverse of this situation occurred in the second area. When the controller performances for the attack magnitudes are analyzed, TI-TD and PI-PD (0.084 p.u.) are the most successful controller, while TID and PID are the least successful for this type of attack.

4 Conclusion

This paper demonstrates the effectiveness of step/stepless and fractional/integer order controllers. We evaluate the performance of PID, TID, PI-PD and TI-TD controllers in stabilizing the frequency and tie-line power of a two-area PV-RT power system. Through the compelling analysis process involved in this study, we prove the significance of our findings.

TDA and RLC are taken into consideration in this study as in the existing studies in the literature. On the other hand, unlike the literature, robustness performances are analyzed within a change of ± 75% for the system parameters, and the limits of system parameters change are discussed. In addition, for this specific power system, C-A performance of the proposed controllers is analyzed for the first time, and also the attack limits are determined. For further analysis, TD, BD, GRC, and GDB are all applied to the system together. The results of this study can be summarized as follows.

- In the PV-RT power system, the TI-TD controller shows by far the best performance for TDA analysis. In PV-RT power system with GDB-GRC/GDB-GRC-BD-TD, the TI-TD and PI-PD controllers show close performance for TDA. In addition, these controllers show superior performance compared to other controllers.
- The robustness analysis is performed for the TI-TD controller due to its superior performance in the PV-RT power system. The controller also performed satisfactorily in this analysis.
- For RLC analysis, all controllers are tested again, and the best results are obtained with the TI-TD controller.
- Among the C-A methods, the TID controller shows the best performance as a result of the attack (ResA) based on information, while cascade (TI-TD/PI-PD) controllers

Table 14 Controller performance for RndA

RndA	TI-TD		PI-PD		TID		PID	
	Area 1	Area 2	Area 1	Area 2	Area 1	Area 2	Area 1	Area 2
RoCoF (Hz/s) for 0.1 p.u	0.1299	1.1874	0.1132	1.1862	0.2936	1.5239	0.2606	1.5394
Max. attack mag. (p.u.)	0.084		0.084		0.065		0.064	

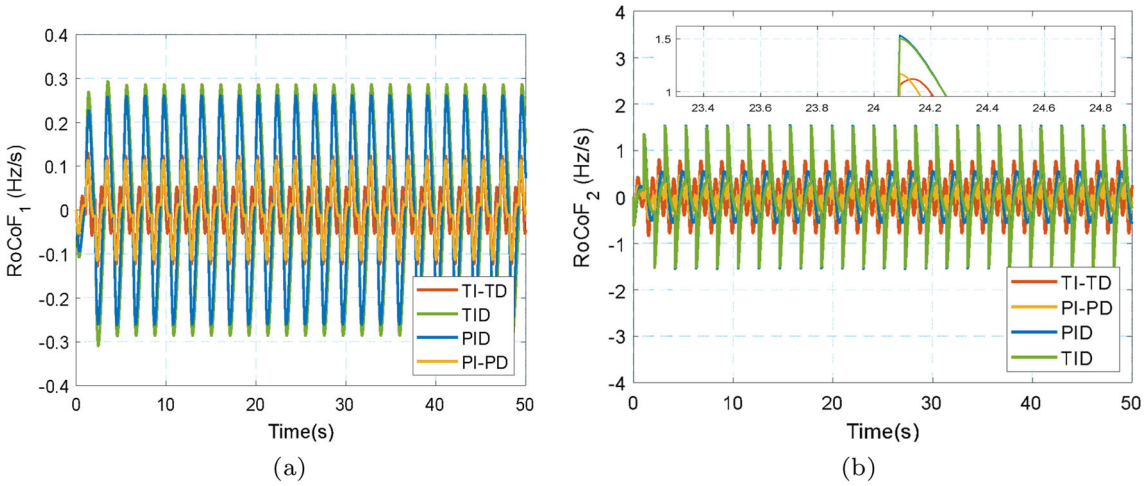


Fig. 11 RoCoF results of power system areas for random attack. **a** Area-1, **b** Area-2

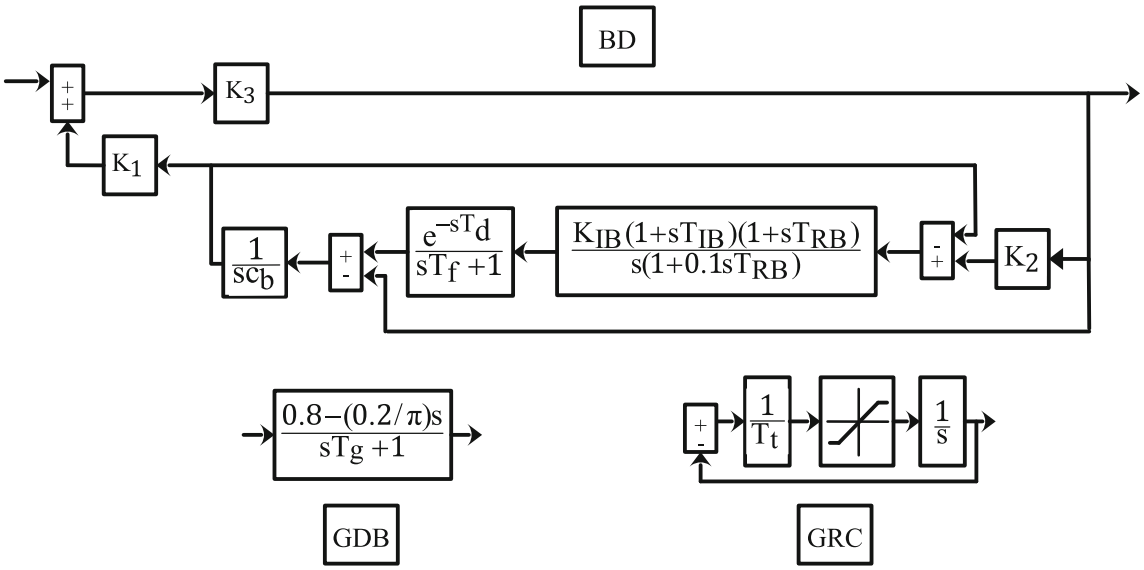


Fig. 12 Model of nonlinear modules

show the best result in the attack (RndA) without information.

In light of the above-given explanations, it can be said clearly that the TI-TD fractional order cascaded controller is the best structure for this system among the considered controllers. As a future work, the performance of the fractional derivative terms may be investigated with and without a derivative filter which can also have fractional or integer order.

Author Contributions BC modeled the case building, performed the experiments and organized whole paper. ES modeled the case building, performed the experiments and organized whole paper. ES modeled the case building, performed the experiments and organized whole paper. OA modeled the case building, performed the experiments and organized whole paper. FMN modeled the case building, performed the experiments and organized whole paper.

Table 15 PV-RT Power System and Boiler Dynamics

PV-RT PS [24]	B=0.8 p.u	R=2.5 Hz/p.u	K_p=120 Hz/p.u	T_g=0.08 s	T_t=0.3 s
	K_r=0.33	a=900	b=-18	c=100	d=50
	T_r=10 s	T_{ps}=20 s	T_{12}=0.545 p.u		
BD [27]	K_1=0.85	K_2=0.095	K_3=0.92	c_b=200	K_{IB}=0.03
	T_{RB}=69 s	T_{IB}=26 s	T_f=10 s	T_d=0	

Funding The authors have not disclosed any funding.

Data availability Enquiries about data and materials availability should be directed to the authors.

Appendix A Methodology

See Table 15.

References

1. Liu F, Li Y, Cao Y, She J, Wu M (2016) A two-layer active disturbance rejection controller design for load frequency control of interconnected power system. IEEE Trans Power Syst 31(4):3320–3321
2. Mohan AM, Meskin N, Mehrjerdi H (2020) A comprehensive review of the cyber-attacks and cyber-security on load frequency control of power systems. Energies 13(15):3860
3. Lamba R, Singla SK, Sondhi S (2019) Design of fractional order PID controller for load frequency control in perturbed two area interconnected system. Electr Power Compon Syst 47(11–12):998–1011
4. Daraz A, Malik SA, Mokhlis H, Haq IU, Laghari GF, Mansor NN (2020) Fitness dependent optimizer-based automatic generation control of multi-source interconnected power system with non-linearities. IEEE Access 8:100989–101003
5. Khadanga Kumar R, Kumar A, Panda S (2020) A novel modified whale optimization algorithm for load frequency controller design of a two-area power system composing of PV grid and thermal generator. Neural Comput Appl 32(12):8205–8216
6. Podlubny I (1999) Fractional-order systems and $PI\lambda D\mu$-controllers. IEEE Trans Autom Control 44(1):208–214
7. Behera SP, Biswal A, Swain B, Samantray SS (2018) Hybrid power systems Frequency regulation using TID based robust controller design and differential evolution (DE) algorithm. In: 2018 Technologies for Smart-City Energy Security and Power (ICSESP), Bhubaneswar, pp 1-6. India
8. Kumar SA, Narayana M, Gowd KJ (2021) Application of TID controller in LFC of two area system under open market scenario, 2nd International Conference on IoT Based Control Networks and Intelligent Systems, July, pp 1-11. India
9. Veerasamy V, Wahab NIA, Ramachandran R, Othman ML, Hizam H, Irudayaraj AXR, Kumar JS (2020) A Hankel matrix based reduced order model for stability analysis of hybrid power system using PSO-GSA optimized cascade PI-PD controller for automatic load frequency control. IEEE Access 8:71422–71446
10. Kumari S, Shankar G (2019) Maiden application of cascade tilt-integral-tilt-derivative controller for performance analysis of load frequency control of interconnected multi-source power system. IET Gener Transm Distrib 13(23):5326–5338
11. Elsaied MM, Abdel Hameed WH, Hasanien HM (2022) Frequency stabilization of a hybrid three-area power system equipped with energy storage units and renewable energy sources. IET Renew Power Gener 16(15):3267–3286
12. Ali T, Malik SA, Hameed IA, Daraz A, Mujlid H, Azar AT (2022) Load frequency control and automatic voltage regulation in a multi-area interconnected power system using nature-inspired computation-based control methodology. Sustainability 14(19):12162
13. Tripathy S, Debnath MK, Kar SK (2023) Optimal design of PI/PD dual mode controller based on quasi opposition based learning for power system frequency control. e-prime-advances in electrical engineering. Electron Energy 4:100135
14. Güler Y, Kaya I (2023) Load frequencycontrol of single-area power system with PI-PD controller design for performance improvement. J Electr Eng Technol 18:2633–2648
15. Çelik E (2021) Design of new fractional order PI-fractional order PD cascade controller through dragonfly search algorithm for advanced load frequency control of power systems. Soft Comput 25(2):1193–1217
16. Elkasem AH, Khamies M, Hassan MH, Agwa AM, Kamel S (2022) Optimal design of TD-TI controller for LFC considering renewables penetration by an improved chaos game optimizer. Fractal Fract 6(4):220
17. Çelik E, Öztürk N, Arya Y, Ocak C (2021) (1+ PD)-PID cascade controller design for performance betterment of load frequency control in diverse electric power systems. Neural Comput Appl 33(22):15433–15456
18. Barakat M, Mabrouk AM, Donkol A (2023) Optimal design of a cascade controller for frequency stability of photovoltaic-reheat thermal power systems considering nonlinearities. Opt Quantum Electron 55(4):295
19. Halmous A, Oubbati Y, Lahdeb M, Arif S (2023) Design a new cascade controller PD-P-PID optimized by marine predators algorithm for load frequency control. Soft Comput 27(14):9551–9564
20. Abou El-Ela AA, El-Sehiemy RA, Shaheen AM, Diab AEG (2021) Enhanced coyote optimizer-based cascaded load frequency controllers in multi-area power systems with renewable. Neural Comput Appl 33:8459–8477
21. Pathak PK, Yadav AK (2023) Design of optimal cascade control approach for LFM of interconnected power system. ISA Trans 137:506–518
22. Choudhary R, Rai JN, Arya Y (2022) Cascade FOPI-FOPTID controller with energy storage devices for AGC performance advancement of electric power systems. Sustain Energy Technol Assess 53:102671
23. Arya Y (2019) AGC of PV-thermal and hydro-thermal power systems using CES and a new multi-stage FPIDF-(1+ PI) controller. Renew Energy 134:796–806
24. Abd-Elazim SM, Sahar M, Ali ES (2018) Load frequency controller design of a two-area system composing of PV grid and thermal generator via firefly algorithm. Neural Comput Appl 30(2):607–616

25. Gozde H, Taplamacioglu MC (2011) Automatic generation control application with craziness based particle swarm optimization in a thermal power system. Int J Elect Power Energy Syst 33(1):8–16
26. Sahin E (2020) Design of an optimized fractional high order differential feedback controller for load frequency control of a multi-area multi-source power system with nonlinearity. IEEE Access 8:12327–12342
27. Guha D, Roy PK, Banerjee S (2018) Symbiotic organism search algorithm applied to load frequency control of multi-area power system. Energy Syst 9(2):439–468
28. Guha D, Roy PK, Banerjee S (2017) Study of differential search algorithm based automatic generation control of an interconnected thermal-thermal system with governor dead-band. Appl Soft Comput 52:160–175
29. Patel NC, Debnath MK, Sahu BK, Dash SS, Bayindir R (2019) Application of invasive weed optimization algorithm to optimally design multi-staged PID controller for LFC analysis. Int J Renew Energy Res 9(1):470–479
30. Topno PN, Chanana S (2018) Differential evolution algorithm based tilt integral derivative control for LFC problem of an interconnected hydro-thermal power system. J Vib Control 24(17):3952–3973
31. Priyadarshani S, Subhashini KR, Satapathy JK (2021) Pathfinder algorithm optimized fractional order tilt-integral-derivative (FOTID) controller for automatic generation control of multi-source power system. Microsyst Technol 27(1):23–35
32. Taher SA, Fini MH, Aliabadi SF (2014) Fractional order PID controller design for LFC in electric power systems using imperialist competitive algorithm. Ain Shams Eng J 5(1):121–135
33. Gheisarnejad M (2018) An effective hybrid harmony search and cuckoo optimization algorithm based fuzzy PID controller for load frequency control. Appl Soft Comput 65:121–138
34. Sahu BK, Pati TK, Nayak JR, Panda S, Kar SK (2016) A novel hybrid LUS-TLBO optimized fuzzy-PID controller for load frequency control of multi-source power system. Int J Electr Power Energy Syst 74:58–69
35. Arya Y (2019) A new optimized fuzzy FOPI-FOPD controller for automatic generation control of electric power systems. J Frankl Inst 356(11):5611–5629
36. Arya Y (2019) Impact of ultra-capacitor on automatic generation control of electric energy systems using an optimal FFOID controller. Int J Energy Res 43(14):8765–8778
37. Sahu RK, Panda S, Biswal A, Sekhar GC (2016) Design and analysis of tilt integral derivative controller with filter for load frequency control of multi-area interconnected power systems. ISA Trans 61:251–264
38. Ranjan M, Shankar R (2022) A literature survey on load frequency control considering renewable energy integration in power system: recent trends and future prospects. J Energy Stor 45:103717
39. Sargolzaei A, Yen KK, Abdelghani MN (2013) Time-delay switch attack on load frequency control in smart grid. Adv Commun Technol 5:55–64
40. Liu S, Liu XP, El Saddik A (2013) Denial-of-Service (dos) attacks on load frequency control in smart grids, In: 2013 ieee pes innovative smart grid technologies conference (isgt), pp 1-6. Washington
41. Wu Y, Wei Z, Weng J, Li X, Deng RH (2017) Resonance attacks on load frequency control of smart grids. IEEE Trans Smart Grid 9(5):4490–4502
42. Zervoudakis K, Tsafarakis S (2020) A mayfly optimization algorithm. Comput Ind Eng 145:106559
43. Gheisarnejad M, Khooban MH (2019) Design an optimal fuzzy fractional proportional integral derivative controller with derivative filter for load frequency control in power systems. Trans Inst Meas Control 41(9):2563–2581
44. Arya Y (2018) Automatic generation control of two-area electrical power systems via optimal fuzzy classical controller. J Frankl Inst 355(5):2662–2688
45. Arya Y (2018) AGC of two-area electric power systems using optimized fuzzy PID with filter plus double integral controller. J Frankl Inst 355(11):4583–4617
46. Khadanga RK, Kumar A, Panda S (2020) A hybrid shuffled frog-leaping and pattern search algorithm for load frequency controller design of a two-area system composing of PV grid and thermal generator. Int Numer Model Electron Netw Devices Fields 33(1):2694
47. Dahiya P, Saha AK (2022) Frequency regulation of interconnected power system using black widow optimization. IEEE Access 10:25219–25236. https://doi.org/10.1109/ACCESS.2022.3155201
48. Davtalab S, Tousi B, Nazarpour D (2022) Optimized intelligent coordinator for load frequency control in a two-area system with PV plant and thermal generator. IETE J Res 68(5):3876–3886. https://doi.org/10.1080/03772063.2020.1782777
49. Khadanga RK, Kumar A, Panda S (2022) A modified grey wolf optimization with cuckoo search algorithm for load frequency controller design of hybrid power system. Appl Soft Comput 124:109011. https://doi.org/10.1016/j.asoc.2022.109011
50. Özay CAN, Eroğlu H, Öztürk A (2023) FV-termal güç sistemlerinde balina optimizasyon algoritması tabanlı otomatik üretim kontrolörü. Gazi Üniversitesi Mühendislik Mimarlık Fakültesi Dergisi 38(2):915–926
51. Padhan S, Sahu RK, Panda S (2014) Application of firefly algorithm for load frequency control of multi-area interconnected power system. Electr Power Compon Syst 42(13):1419–1430
52. Tan W, Chang S, Zhou R (2017) Load frequency control of power systems with non-linearities. IET Gener Transm Distrib 11(17):4307–4313
53. Haroun AG, Li YY (2017) A novel optimized hybrid fuzzy logic intelligent PID controller for an interconnected multi-area power system with physical constraints and boiler dynamics. ISA Trans 71:364–379
54. Jagatheesan K, Anand B, Baskaran K, Dey N, Ashour AS, Balas VE (2018) Effect of nonlinearity and boiler dynamics in automatic generation control of multi-area thermal power system with proportional-integral-derivative and ant colony optimization technique. In: Recent advances in nonlinear dynamics and synchronization. pp 89-110. Springer
55. Guha D, Roy PK, Banerjee S (2018) Application of backtracking search algorithm in load frequency control of multi-area interconnected power system. Ain Shams Eng J 9(2):257–276
56. Arya Y, Kumar N (2017) BFOA-scaled fractional order fuzzy PID controller applied to AGC of multi-area multi-source electric power generating systems. Swarm Evolut Comput 32:202–218
57. Sahu RK, Panda S, Padhan S (2015) A novel hybrid gravitational search and pattern search algorithm for load frequency control of nonlinear power system. Appl Soft Comput 29:310–327
58. Guha D, Roy PK, Banerjee S (2016) Load frequency control of interconnected power system using grey wolf optimization. Swarm Evolut Comput 27:97–115
59. Kargar HK, Mirzaei J (2008) New method for islanding detection of wind turbines. In: 2008 IEEE 2nd International Power and Energy Conference, pp. 1633-1637
60. Chen YQ, Petras I, Xue D (2009) Fractional order control - A tutorial American Control Conference, pp 1397-1411. USA
61. Wiora J, Wiora A (2020) Influence of methods approximating fractional-order differentiation on the output signal illustrated by three variants of oustaloup filter. Symmetry (Basel) 12(11):1–19
62. Xue D, Zhao C, Chen YQ (2006) A modified approximation method of fractional order system, In:2006 IEEE International Conference on Mechatronics and Automation, ICMA 2006, pp 1043-1048. China

63. Bingi K, Ibrahim R, Karsiti MN, Hassam SM, Harindran VR (2019) Frequency response based curve fitting approximation of fractional-order PID controllers. Int J Appl Math Comput Sci 29:311–326
64. Xue D, Chen Y, Atherton D (2007) Linear Feedback Control: Analysis and Design with MATLAB. Society for Industrial and Applied Mathematics, Philadelphia
65. Bhattacharyya T, Chatterjee B, Singh PK, Yoon JH, Geem ZW, Sarkar R (2020) Mayfly in harmony: a new hybrid meta-heuristic feature selection algorithm. IEEE Access 8:195929–195945
66. Jacobus LM, Macadam CR, Sartori M (2019) Mayflies (Ephemeroptera) and their contributions to ecosystem services. Insects 10(6):170
67. Abd Elaziz M, Senthilraja S, Zayed ME, Elsheikh AH, Mostafa RR, Lu S (2021) A new random vector functional link integrated with mayfly optimization algorithm for performance prediction of solar photovoltaic thermal collector combined with electrolytic hydrogen production system. Appl Therm Eng 193:117055
68. Gao ZM, Zhao J, Li SR, Hu YR (2020) The improved mayfly optimization algorithm. In: Journal of Physics: Conference Series, IOP Publishing, Shanghai, 1684(1), pp. 012077. China
69. Shaw B, Nayak JR, Sahu R (2020) Implementation of hDE-HTS optimized T2FPID controller in solar-thermal. Data management analytics and innovation system. Springer, Singapore, pp 401–412
70. Morsali J, Zare K, Hagh MT (2014) Appropriate generation rate constraint (GRC) modeling method for reheat thermal units to obtain optimal load frequency controller (LFC), In: 2014 5th Conference on Thermal Power Plants (CTPP),IEEE, pp. 29-34. Iran

Publisher's Note Springer Nature remains neutral with regard to jurisdictional claims in published maps and institutional affiliations.

Springer Nature or its licensor (e.g. a society or other partner) holds exclusive rights to this article under a publishing agreement with the author(s) or other rightsholder(s); author self-archiving of the accepted manuscript version of this article is solely governed by the terms of such publishing agreement and applicable law.